Large Electric Field–Enhanced–Hardness Effect in a SiO$_2$ Film

Reynier I. Revilla, Xiao-Jun Li, Yan-Lian Yang & Chen Wang

CAS Key Laboratory of Standardization and Measurement for Nanotechnology, National Center for Nanoscience and Technology, Beijing 100190, P. R. China.

Silicon dioxide films are extensively used in nano and micro–electromechanical systems. Here we studied the influence of an external electric field on the mechanical properties of a SiO$_2$ film by using nanoindentation technique of atomic force microscopy (AFM) and friction force microscopy (FFM). A giant augmentation of the relative elastic modulus was observed by increasing the localized electric field. A slight decrease in friction coefficients was also clearly observed by using FFM with the increase of applied tip voltage. The reduction of the friction coefficients is consistent with the great enhancement of sample hardness by considering the indentation–induced deformation during the friction measurements.

With the rapid development of nano and micro–electromechanical systems (NEMS/MEMS), it becomes genuinely important to gain insight on the effects of high electric fields on friction and mechanical properties of materials (such as the Young's modulus) at nanometer and micrometer scale. Electric field has previously shown to affect the mechanical properties of a number of materials[1–4], and various outcomes have been obtained. The ductility of the Al–Li alloy was improved, while the strength properties remained approximately the same under the influence of an external electric field[1]. Due to the fact that there is no electric field in the interior of the bulk metal, according to the electric field theory, the authors have proposed that the electric field decreases the density of the alloy valence electrons. This could reduce the alloy internal energy, and hence improve ductility. It has also been observed that electric field affects the mechanical strength of poled lead zirconate titanate (PZT), one of the most widely used piezoelectric ceramic materials[2]. A decrease and a sharp increase of the PZT strength were detected depending on the polarity and magnitude of the applied electric field (electric field ranging between −40 and 40 kV/cm). The authors have associated the variations observed in the mechanical strength with dipoles or domain switching and the amount of switchable domains. They claimed that the effectiveness and degree of induced domain switching is closely related to the electric field–toughening effect. In a different work, by using nanoindentation technique, local softening was noted in another well known piezoelectric material, zinc sulfide (ZnS) crystals, caused by the application of an external electric field (maximum field intensity was 20 V/cm)[3]. The authors considered that the electric field increases the average velocity of the charged dislocations and changes the electromechanical interaction, which in turn affects indentation hardness. Furthermore, a recently published work has presented a nanoporous metal immersed in an electrolyte in which strength and ductility can be tuned by polarizing the internal interface via an applied electric potential[4]. Even though the effect observed is not exactly caused by the electric field strength, this work is of great significance while studying materials with electrically tunable mechanical properties.

Previous works studying the influence of electric field on the mechanical properties of a number of materials have shown a great variety of explanations, depending on the specific system. This supports the necessity for more rigorous studies on the influence of electric field on the mechanical properties of various materials, especially those frequently affected by external electric fields.

Particularly, silicon dioxide (SiO$_2$) films are widely used in the micro–electronic industry, in NEMS and MEMS. Several studies have been reported to determine the hardness and elastic modulus of SiO$_2$ films[5–8], but none has considered the effect of external electric field on its mechanical properties.

Force spectroscopy method of atomic force microscopy (AFM) has been widely used in the past decade to study mechanical properties of materials by using nanoindentation techniques[9,10]. Examples include biological samples[11–17], membranes[18,19] and ceramic materials[20–22], among others. In addition, friction force microscopy (FFM), phase imaging and the quantitative nanomechanical property mapping are also well known powerful tools for surface analysis, which can provide nanoscale morphology with high spatial resolution and rich information, such as surface chemical composition, molecular organization and mechanical properties, among others. The latter

two techniques are more advanced and informative for heterogeneous materials and films, while for homogeneous materials with nearly uniform surface properties they could not present their superiorities. FFM methods are more convenient and straightforward for mechanical property and surface property studies.

In the present work, by using nanoindentation technique and friction force microscopy we studied the influence of an external electric field on the mechanical properties of a SiO_2 film. By applying voltage to a conductive AFM probe and using the substrate as the bottom electrode, tip–sample elastic modulus experienced a great increase. This outcome could be associated with polarization within the SiO_2 film due to the electric field produced by the tip voltage. Friction coefficient was observed to decrease by raising the electric field, which seems to be in agreement with the enhanced film hardness.

Results

To investigate the deformation process we first identified the indentation range and the limits of the loading force, using a procedure similar to the one described by Sun et al.[23]. Fig. 1a shows the loading and unloading curves (cantilever deflection, x, vs piezoelectric drive distance, z_p) obtained for SiO_2 with tip bias equals to zero (loading and unloading forces are represented as cantilever deflection, in any case they are proportional magnitudes), using a conductive silicon tip with a coating of a 3 nm–Cr and 20 nm–Pt-Ir
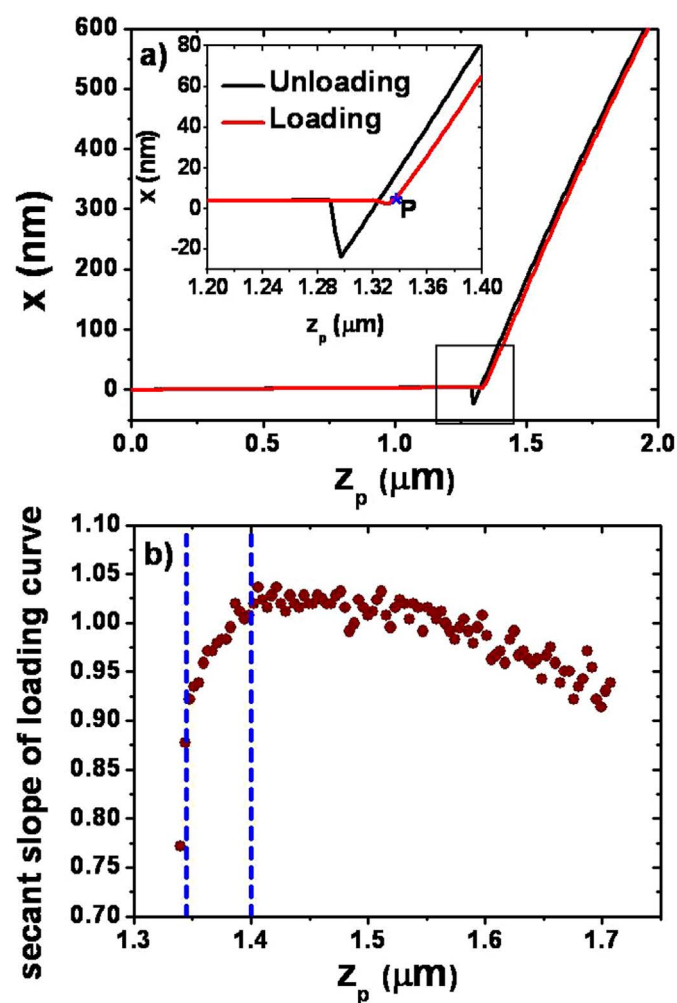

Figure 1 | Force–curve and secant slope of the loading part at 0 V tip bias. (a) Loading–unloading curve for SiO_2 with a tip bias of 0 V. (b) Secant slope of the loading curve in Fig. 1a from the zero deflection signal point (zero load signal) to the subsequent deflection signal.

film. The secant slope of the loading curve in Fig. 1a is presented in Fig. 1b from the point P in Fig. 1a (zero deflection signal point) to subsequent deflection signal (determination of point P is explained in method section). It can be observed that only for z_p in the range of 1350–1400 nm the loading curve affects indent deformation. For z_p values greater than 1400 nm the secant slope is approximately constant, which means the indentation depth can be neglected because almost all the piezo movement (z_p) is converted to cantilever deflection (x). In Fig. 1a it can be noted that for $z_p = 1400$ nm, cantilever deflection is approximately 65 nm. By repeatedly conducting this measurement, we corroborated that the maximum cantilever deflection for which we would have a distinguishable sample deformation was $x \approx 65$ nm. In order to avoid damage in the sample surface, the maximum cantilever deflection was kept lower than 60 nm. The same measurement and analysis was made in the same sample (SiO_2 with 550 nm thickness) for a tip bias of 9 volts, which roughly represents an electric field of approximately 164 kV/cm according to the procedure described in the method section. No noticeable variation in the secant slope of the loading curve could be identified as it can be seen in the supporting information (Fig. S1). This is a typical behavior of rigid samples and clearly shows a variation in the mechanical properties caused by the application of an external electric field. The same behavior was observed for electric field values higher than 164 kV/cm.

Fig. 2 portrays the cantilever deflection versus the nominal separation measured during loading the SiO_2 film at different applied electric field. Curves were taken in the same sample location while increasing the tip bias. The photodetector sensitivity was updated to the average sensitivity values of the force curves obtained for 9 volts after recorded ($\sim$164 kV/cm). The reason for that is because no perceptible deformation was observed by analyzing the loading curve secant slope at 164 kV/cm (see Fig. S1 of supporting information). Therefore, nearly all the piezo movement is converted to cantilever deflection in that case, which is suitable for the sensitivity calibration. As it can be noted in Fig. 2, the sample deformation (negative values of the nominal separation) decreases by increasing the applied electric field, which means an increase in the sample hardness by increasing the tip bias. This is in agreement with the fact that noticeable variations were observed in the loading curve secant slope at 0 V (Fig. 1) but no for 9 V (164 kV/cm) (Fig. S1).

In order to reveal the elastic properties from the force spectroscopy method, the Derjaguin–Müller–Toporov (DMT) model[24,25] was used for simplicity. According to this model the loading force (F_{load}) is related to the sample deformation (δ) through the equation (1):
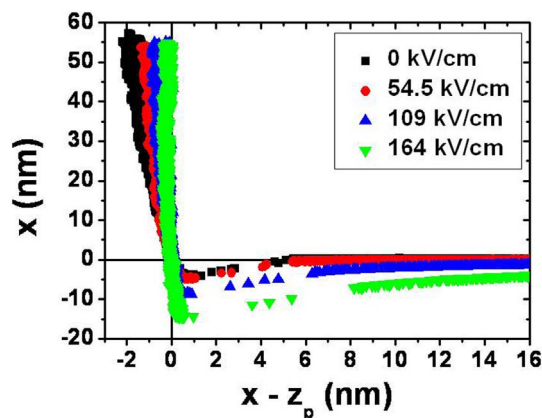

Figure 2 | Cantilever deflection versus nominal separation at different tip bias. Cantilever deflection versus nominal separation obtained while loading the SiO_2 surface for different values of the tip bias. Five loading curves are portrayed for every value of the applied electric field.

$$F_{load} = \frac{4}{3} E^* R^{1/2} \delta^{3/2} + F_{adh} \qquad (1)$$

where E^* is the reduced elastic modulus of the tip and the sample, R is the tip radius, and F_{adh} is the adhesion force during the contact. In equation (1) the indenter is considered as a paraboloid of revolution.

In order to estimate the reduced elastic modulus, F_{load} vs δ plots were fitted by equation (1). The loading force was obtained by multiplying the cantilever deflection by its spring constant, and the deformation was the absolute value of the negative part of the nominal separation. In Fig. 2 it can also be observed that the maximum deformation experienced during the indentation process is about 1.8 nm. Thus, the value of R used in equation (1) is the average radius at 1.8 nm from the tip apex ($R = 2.6$ nm), which was obtained using the NanoScope Analysis software and a standard Tip Check sample. No fitting was made for the curve at 164 kV/cm because those data were used to calibrate the photodetector sensitivity, and thus, no deformation was considered in that case. The tip–sample's reduced elastic modulus was estimated for different values of the applied electric field. Values are listed in Table 1.

Parallel to this, it is well known that the reduced modulus is related to the elastic modulus through the following equation:

$$\frac{1}{E^*} = \frac{1 - v_s^2}{E_s} + \frac{1 - v_i^2}{E_i} \qquad (2)$$

where, E_i and v_i are Young's modulus and Poisson's ratio of the indenter, and E_s and v_s are those of the sample. In our case the indenter is a silicon cantilever with 20 nm Pt–Ir coating. Effective mechanical properties of layered surfaces is a complex topic that has only been solved for few and very specific systems[26]. Since Pt–Ir elastic modulus is much larger than the sample's modulus and no considerable variation in the tip apex was observed after the measurement, we have considered Pt–Ir elastic properties as the indenter parameters in order to simplify the model and calculations. Even though this is a rough approximation, the results showed good agreement among each other as it is shown below. Table S1 in the supporting information shows the elastic properties of the materials implicated in the indentation process. By using equation (2), E^* is obtained to be ranging between 51.9 and 58 GPa. It can be noted that the value of E^* at zero external electric field obtained using equation (1) (55.1 GPa, see Table 1) is in good agreement with the reduced modulus estimated with equation (2) using parameters reported in the literature (table S1 of supporting material).

In addition, to further confirm the electric field effect in the elastic modulus, the same experiment was carried out on a SiO_2 film with different thickness (450 nm) using a conductive AFM tip from the same batch (silicon cantilever with a coating of a 3 nm–Cr and 20 nm–Pt-Ir film). After applying the same procedure described above, the reduced elastic modulus for different values of the external applied electric field were estimated. Results are shown in Fig. 3. Figure 3b shows a comparison with those obtained using a 550 nm thick SiO_2 film. It can be observed that the tip–sample elastic modulus greatly increases by increasing the external electric field following a similar behavior to the one obtained for the 550 nm thick SiO_2 film. The comparison with other much thinner SiO_2 films will definitely provide more insight in understanding the electric field effect on the

mechanical properties of this system. However, the comparison of the results with two thicknesses indicates that the electric field effects on the elastic modulus of the thinner film (450 nm) are less pronounced than that of the thicker film (550 nm). In addition, substrate effect may become more significant as the thickness is reduced, which is not favorable in the experimental conditions. The value of E^* at zero external electric field was obtained to be 62.2 GPa using equation (1). This value is also in very good agreement with the reduced modulus predicted with equation (2).

Additionally, friction force microscopy was also conducted under the effect of external electric field in order to provide additional information about the influence of the electric field on the mechanical properties of the SiO_2 film at nanoscale. Fig. 4a shows, for different values of the applied voltage, the photo–detector response (friction signal, FS) as a function of the applied load. The relationship between FS and the load is approximately linear. This linearity suggests that the data is in agreement with Derjaguin's modified version of Amontons' law[27], which includes the contribution from adhesion forces:

$$F_f = \mu(F_L + F_{adh}) \qquad (3)$$

where F_f and F_L are the friction force and the applied load respectively, μ is the friction coefficient, and F_{adh} is associated with the total adhesive force. Equation (3) has been widely used in the literature to study frictional behavior at nanoscale for systems in which the photo–detector response increases linearly with respect to the applied load.

The data shown in Fig. 4a was fitted using equation (3). Fitting results are shown in Table 2 and plotted in Fig. 4a together with the data points. In the FFM measurement, photo–detector response (friction signal, FS) is a magnitude proportional to the friction force (F_f). To compare friction coefficients from different tip bias, slopes of FS–load plots were used and a normalization procedure was carried out as described in the method section. The results are shown in Fig. 4b. The value of μ showed a slight decrease by increasing the external applied electric field. Friction coefficient at 218 kV/cm fell to approximately 76% of the value at zero external electric field. As it has been explained before, the friction coefficients obtained in this work are relative values. Even if they cannot be compared with absolute values, we observed excellent reproducibility when comparing them among each other.

The variation detected in the surface friction could possibly be associated with the differences observed in the elastic modulus. If the Young's modulus, which is a measure of sample stiffness, is relatively low, indentation–induced–deformation is more likely to occur while loading and sliding the tip onto the sample surface. This deformation might create a local wrinkle, as shown in Fig. 5a, and consequently increase the tip–sample contact area. The enlarged contact area as a result of the deformation requires more force to slide the tip forward. When the elastic modulus is increased by the application of an external electric field, pleating effect is less prominent (less likely to occur), and therefore friction is lower (Fig. 5b). The slight decrease of friction coefficients, as can be seen in Fig. 4b, is in qualitative agreement with this possible pleating effect.

Discussion

The increase of tip–sample elastic modulus by increasing the voltage applied to the tip (see Table 1) is an interesting outcome that has not been observed before. The nanometer scale distance between the biased tip and the sample gives rise to a very high electric field ($\sim$164 kV/cm at 9 V). This field could polarize the dipoles within the molecular structure of the SiO_2 film, in the region below the tip apex. The sample polarization density (P_s), in general responds non-linearly to the applied electric field, in which several order susceptibilities are present. The nonlinearity phenomenon is typically only observed at very high values of the electric field ($\sim10^3$ kV/cm),

Table 1 | Value of the reduced elastic modulus obtained from fitting the loading force values versus deformation under different tip bias using DMT model

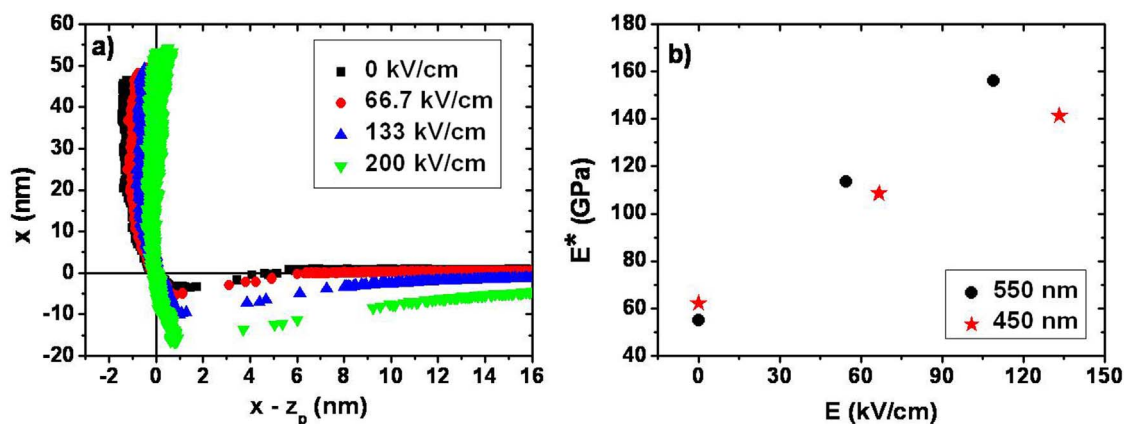| Tip bias (V)	E (kV/cm)	4 (E*R^½)/3	E* (GPa)
0	0	118.4	55.1
3	54.5	243.9	113.4
6	109	335.7	156.1

Figure 3 | **Cantilever deflection versus nominal separation at different tip bias for a film with a thickness of 450 nm and comparison between the reduced elastic modulus calculated for two different film thicknesses.** (a) Cantilever deflection versus nominal separation obtained while loading a 450 nm thick SiO_2 film for different values of the tip bias. Five loading curves are portrayed for every value of the applied electric field. (b) Reduced elastic modulus obtained for 450 and 550 nm thick SiO_2 films.

partially due to the much smaller nonlinear dielectric constant compared to the linear one. The linear part of the polarization density, which is the prevailing term in this case, is proportional to the sample susceptibility (χ_s) and the electric field from the biased tip (E), which in turn is proportional to the voltage applied to the tip (V). In general, the polarization density could be expressed as:

$$P_s = P_{s0} + \varepsilon_o \chi_s E + \Phi\left(\chi^{(n)}, E\right)$$
$$= P_{s0} + \varepsilon_o \chi_s h_{t-s} V + \Phi\left(\chi^{(n)}, V\right) \tag{4}$$

where h_{t-s} is a factor related to the tip–sample geometry, P_{s0} is the permanent sample polarization density and Φ is a function that accounts for the nonlinearity contribution.

Increasing the tip bias increases the polarization density, and consequently could also come into play an additional term in the inter–particle forces, which could be associated with dipole–dipole interaction:

$$f_i^{\alpha\beta} = f_i^{\alpha\beta}{}_{E=0} + ag^{\alpha\beta}\left(p^\alpha p^\beta\right)_i \approx f_i^{\alpha\beta}{}_{E=0} + ag^{\alpha\beta}\left(p^\alpha\right)_i^2 \tag{5}$$

where a is a constant, $f_i^{\alpha\beta}$ is the inter–particle force (along direction i) applied on particle α by particle β (i takes values of x, y and z directions), p^α (p^β) is the electric dipole moment of particle α (β), $g^{\alpha\beta}$ is a magnitude related to the inter–particle distance ($r^{\alpha\beta}$) and the relative orientation of dipoles α and β. As it can be seen in table S2 of the

supporting information, depending on the dipoles orientation, very different values of the interaction energy can be obtained. If the dipole moments are more or less co–orientated and perpendicular to the line joining their centers, strong repulsion occurs among them. On the contrary, if they are co–orientated and parallel to the line joining their centers, an attractive force arises between them.

In addition, it is well known that mechanical stress at the atomic and molecular level (see virial stress in the supporting information) is proportional to the inter–particle forces, explicitly to the combination of all the inter–particle interactions within a confine volume. Consequently, in order to estimate local stress (σ_{ij}) under the influence of an external electric field, the additional term associated with dipole–dipole interaction in equation (5) could also be taken into account. This might originate a new term, very complex, which will depend on the exact relative orientation of the dipole moments. That additional term should be zero in the absence of dipole polarization. Therefore, as a first approximation, the local mechanical stress could be predicted as:

$$\sigma_{ij} \approx \sigma_{ij_{E=0}} + a_{ij} P_s^2 = \sigma_{ij_{E=0}} + \Gamma_{ij}(E) \tag{6}$$

a_{ij} is a constant. Function Γ has information of particle orientation and the electric field strength, including the linear part of the polarization density and the nonlinearity effect (see equation 4). These extra terms, as a consequence of the influence of an external electric field could, accordingly, also affect the magnitude of the local
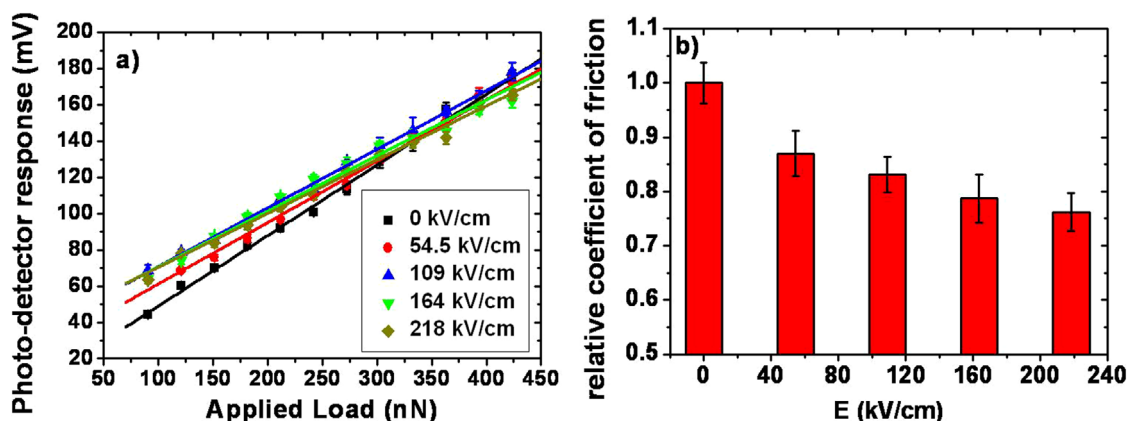

Figure 4 | **Photodetector response vs applied load and relative friction coefficients vs applied voltage.** (a) Photodetector response as a function of the applied load obtained from the friction measurement in the SiO_2 surface. (b) Normalized friction coefficients versus the external applied electric field. Friction coefficients were determined from the slopes of photodetector signal–load plots shown in (a).

Table 2 | Parameter values obtained from fitting the FS–load plots under different external applied voltage with equation (2)

Tip Bias (V)	E (kV/cm)	Slope	Intercept	Adj R–square
0	0	0.390	9.89	0.996
3	54.5	0.339	27.18	0.991
6	109	0.324	38.33	0.995
9	164	0.307	39.93	0.984
12	218	0.297	40.59	0.992

stiffness (c_{ij}), which, as it is known, is closely related to the stress and the strain (ε_{ij}) ($\sigma_{ij} = c_{ijkl}\varepsilon_{kl}$, c_{ijkl} is sometimes written as c_{ij} for convenience). Hence, c_{ij} might be, in general, also a function of the external applied electric field:

$$c_{ij} = c_{ij_{E=0}} + \Gamma'_{ij}(E) \qquad (7)$$

Equations (6) and (7) are just possible approximations to explain the enormous increase in sample's stiffness detected in our experiments. A rigorous study of the local mechanical stress (see virial stress in supporting information) under the influence of an external electric field would require a very thorough analysis of dipoles orientation, which is determined by the exact tip and sample geometry, among other parameters.

In summary, the effects of an external electric field on the mechanical properties of a silicon dioxide film were studied by using nanoindentation technique and friction force microscopy. Experimental data showed a huge increase in the tip–sample elastic modulus and a slight decrease in the tip–sample friction coefficient by increasing the applied tip bias. These two phenomena could be closely related if indentation–induced deformation is taken into consideration during friction force measurements. The improvement of sample hardness by increasing the tip bias might be associated with molecular polarization within the SiO_2 film. This proposition is based on the possible augmentation of the internal mechanical stress due to an additional term related to dipole–dipole interactions. Nevertheless, what actually takes place at this scale during the tip–sample interaction is still beyond our understanding. Additional systematic studies are needed for a better understanding of these phenomena at nanometer scale.

Methods

Samples. A 550 nm thick film of silicon dioxide was deposited on silica (SiO_2/Si(100)) by using physical vapor deposition (PVD). Si(100) used was doped with phosphorus (2–4 $\Omega\cdot$cm) (from Silicon Quest Int'l) and used as the bottom electrode. PVD was carried out by E–beam deposition on a BOC AUTO 500 system, with a base vacuum of 1.6×10^{-6} mbar, E–beam gun electric current of 7 mA and a deposit rate of 0.6 Å/s.

AFM measurements. The measurements were conducted with a commercial AFM (Dimension 3100, Nanoman II, Bruker). A conductive silicon tip with a coating of a 3 nm–Cr and 20 nm–Pt–Ir film and a spring constant of 6.37 N/m was used for the measurements and as the top electrode. Fig. S2 of the supporting material portrays the experimental setup used during the measurements, in which can be noted that the conductive substrate supporting the dielectric film acts as the bottom electrode. The cantilever spring constant was measured from the thermal spectra of the cantilever response by considering this as a harmonic oscillator driven by thermal noise. In order to ensure that the voltage applied to the tip does not cause significant variations in the effective cantilever spring constant, this was measured for different values of the tip bias (see Fig. S3 of supporting material). By increasing the applied voltage up to 10 V, increases the measurement error, probably caused by electronic noises, but the average value of the spring constant remains approximately the same for that range of voltage applied to the tip. The photodetector sensitivity was first calibrated by measuring a force–distance curve on the SiO_2 substrate (photodetector sensitivity is the gradient at the repulsive region), and updated after the measurements using the average of the sensitivity values of the force curves obtained at the higher voltage applied to the tip as the reference.

During the indentation process, force–distance curves were recorded. Fig. S4 in the supporting information shows an example of AFM force data obtained by bringing the tip into contact with a non rigid sample. When the AFM tip is far from the sample surface, there is no interaction between the tip and the surface, and hence no
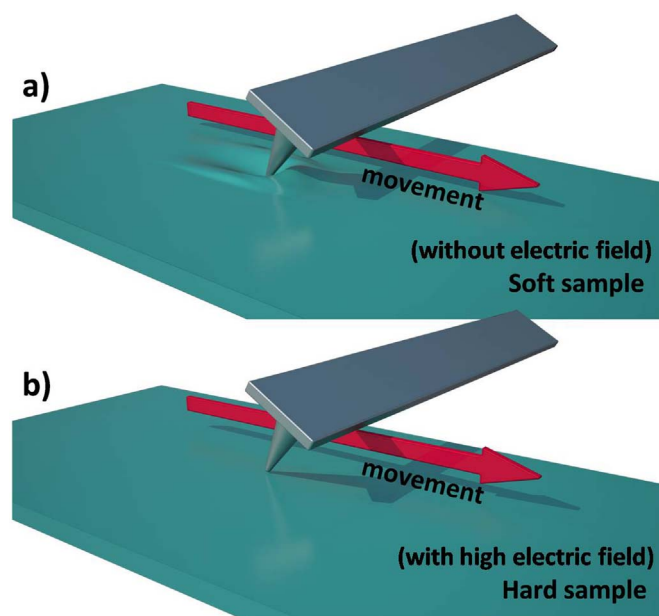
Figure 5 | Representation of possible pleating effect while sliding the tip over the sample surface at different tip bias. Schematic showing the proposed pleating effect probably caused by the tip deforming the sample while sliding over it. This out–of–plane deformation might increase the contact area and friction between tip and sample surface. (a) In a relatively soft sample (in this case representing the system at 0 tip bias). (b) In a relatively hard sample, where the pleating effect is considerable reduced (in this case representing the system under the influence of an external electric field).

cantilever deflection, x ($x \approx 0$) (see Fig. S4a). As the AFM probe moves towards the sample, driven by the piezo movements, a process known as jump–into–contact takes place, and the cantilever bends downwards due to van der Waals, water meniscus and electrostatic interactions, bringing the tip into contact with the sample. As the piezo continues moving, the cantilever deflection increases and the sample is compressed, causing local deformation when is not rigid. The force or applied load can be obtained multiplying the cantilever deflection by its spring constant, k, $F = kx$. The nominal separation is the deflection minus the drive distance (z_p) (see Fig. S3b), $z = x - z_p + const$[28]. The constant represents the choice of the zero of separation. For rigid surfaces the separation is never negative, and the zero corresponds to the position where the force curve becomes vertical. In the case of deformable surfaces the choice of zero is much more problematic. To investigate indentation deformation, some authors consider the zero at the zero deflection signal point after the jump–into–contact[23], point P in the inset of Fig. S4b in the supporting material. Negative values of the nominal separation correspond to the amount of deformation that has occurred.

A series of 5 force curves were obtained for each external voltage applied to the tip on the same sample location (sample was always grounded). To avoid structural damage of the sample the tip was slowly driven while approaching and retracting from the sample surface, the loading and unloading speed was 0.25 μm/s. The probe radius was measured using the NanoScope Analysis software and a standard Tip Check sample (Aurora NanoDevices Inc.), which are commonly used to obtain accurate reconstructions of the tip apex. The probe radius was measured before and after each test in order to ensure that the tip apex did not change due to plastic deformation, which would invalidate the measurement of the Young's modulus. Measurements were made at a relative humidity below 20%, in order to reduce any influence from the possible water condensation in the sample surface.

During the friction measurements, the scanning direction was fixed perpendicular to the long axis of the cantilever beam. As it is known, the magnitude of the friction force is proportional to the degree of torsion of the cantilever, which gives rise to a differential signal in the photodetector given in units of millivolts. The sample was scanned using the same kind of tip as the one used during the force spectroscopy measurement and for different values of the voltage applied to the tip. Under the same potential condition 100 sample lines with trace and retrace per line were recorded in order to obtain the average photodetector response signal. Due that the photodetector may not be properly aligned with respect to the laser beam, the friction signal for each sample line was calculated as the average between the absolute values of the trace and the retrace signal. The final value of the friction signal associated with a specific value of the applied voltage is the average of the friction signal values of the 100 sample lines. Applied load was obtained by multiplying the cantilever spring constant, the photodetector sensitivity and the difference between the deflection set point and the deflection signal when the tip is in its free state. By varying the normal load applied to

the tip, it is possible to construct friction–load plots. The gradients of the friction load plots were used to obtain relative friction coefficients, which were normalized with respect to the highest friction coefficient value obtained.

The electric field strength is estimated as $E = V/d$ (rough estimation as a parallel plate capacitor), where V is the external applied voltage and d the SiO_2 film thickness. In any case, E is a magnitude proportional to the applied voltage.

1. Liu, B., Chen, Z., Wang, Y. & Wang, X. The effect of an electric field on the mechanical properties and microstructure of Al–Li alloy containing Ce. *Mater. Sci. Eng. A* **313**, 6–74 (2001).
2. Wang, H., Lin, H.-T. & Wereszczak, A. A. Strength properties of poled lead zirconate titanate subjected to biaxial flexural loading in high electric field. *J. Am. Ceram. Soc.* **93**, 2843–2849 (2010).
3. Yang, F. & Dang, H. Effect of electric field on the nanoindentation of zinc sulfide. *J. Appl. Phys.* **105**, 056110 (2009).
4. Jin, H. J. & Weissmüller, J. A material with electrically tunable strength and flow stress. *Science* **332**, 1179–1182 (2011).
5. Chu, J. & Zhang, D. Mechanical characterization of thermal SiO_2 micro–beams through tensile testing. *J. Micromech. Microeng.* **19**, 095020 (2009).
6. Gaspar, J., Gualdino, A., Lemke, B., Paul, O., Chu, V. & Conde, J. P. Mechanical and piezoresistive properties of thin silicon films deposited by plasma–enhanced chemical vapor deposition and hot–wire chemical vapor deposition at low substrate temperature. *J. Appl. Phys.* **112**, 024906 (2012).
7. Li, H. & Vlassak, J. J. Determining the elastic modulus and hardness of an ultra–thin film on a substrate using nanoindentation. *J. Mater. Res.* **24**, 1114–1126 (2009).
8. Carlotti, G., Doucet, L. & Dupeux, M. Elastic properties of silicon dioxide films deposited by chemical vapour deposition from tetraethylorthosilicate. *Thin Solid Films* **296**, 102–105 (1997).
9. Clifford, C. A. & Seah, M. P. Quantification issues in the identification of nanoscale regions of homopolymers using modulus measurement via AFM nanoindentation. *Appl. Surf. Sci.* **252**, 1915–1933 (2005).
10. Withers, J. R. & Aston, D. E. Nanomechanical measurements with AFM in the elastic limit. *Adv. Colloid Interface Sci.* **120**, 57–67 (2006).
11. Li, Q. S., Lee, G. Y. H., Ong, C. N. & Lim, C. T. AFM indentation study of breast cancer cells. *Biochem. Biophys. Res. Commun.* **374**, 609–613 (2008).
12. Jandt, K. D. Atomic force microscopy of biomaterials surfaces and interfaces. *Surf. Sci.* **491**, 303–332 (2001).
13. Touhami, A., Nysten, B. & Dufrêne, Y. F. Nanoscale mapping of the elasticity of microbial cells by atomic force microscopy. *Langmuir* **19**, 4539–4543 (2003).
14. Vinckier, A. & Semenza, G. Measuring elasticity of biological materials by atomic force microscopy. *FEBS Lett.* **430**, 12–16 (1998).
15. Kurland, N. E., Drira, Z. & Yadavalli, V. K. Measurement of nanomechanical properties of biomolecules using atomic force microscopy. *Micron* **43**, 116–128 (2012).
16. Sweers, K., van der Werf, K., Bennink, M. & Subramaniam, V. Nanomechanical properties of α–synuclein amyloid fibrils: a comparative study by nanoindentation, harmonic force microscopy, and peakforce QNM. *Nanoscale Res. Lett.* **6**, 270 (2011).
17. Vapaavuori, J., Mahimwalla, Z., Chromik, R. R., Kaivola, M., Priimagi, A. & Barrett, C. J. Nanoindentation study of light–induced softening of supramolecular and covalently functionalized azo polymers. *J. Mater. Chem. C* **1**, 2806–2810 (2013).
18. Franceschini, E. A. & Corti, H. R. Elastic properties of nafion, polybenzimidazole and poly [2,5–benzimidazole] membranes determined by AFM tip nano–indentation. *J. Power Sources* **188**, 379–386 (2009).
19. Lee, C., Wei, X., Kysar, J. W. & Hone, J. Measurement of the elastic properties and intrinsic strength of monolayer graphene. *Science* **321**, 385–388 (2008).
20. Roa, J. J., Oncins, G., Dias, F. T., Vieira, V. N., Schaf, J. & Segarra, M. AFM as an alternative for Young's modulus determination in ceramic materials in elastic deformation regime. *Physica C* **471**, 544–548 (2011).
21. Korobko, R., Kim, S. K., Kim, S., Cohen, S. R., Wachtel, R. & Lubomirsky, I. The role of point defects in the mechanical behavior of doped ceria probed by nanoindentation. *Adv. Funct. Mater.* **23**, 6076–6081 (2013).
22. Zhang, Y., Allahkarami, M. & Hanan, J. C. Measuring residual stress in ceramic zirconia – porcelain dental crowns by nanoindentation. *J. Mech. Behav. Biomed. Mater.* **6**, 120–127 (2012).
23. Sun, C., Su, D. C. & Li, X. D. Investigation of loading and force sensing properties of a probe–type microforce sensor with force–distance curves. *Sci. China Tech. Sci.* **54**, 1362–1370 (2011).
24. Derjaguin, B. V., Müller, V. M. & Toporov, Y. P. Effect of contact deformations on adhesion of particles. *J. Colloid Interface Sci.* **53**, 314–326 (1975).
25. Trtik, P., Kaufmann, J. & Volz, U. On the use of peak–force tapping atomic force microscopy for quantification of the local elastic modulus in hardened cement paste. *Cem. Concr. Res.* **42**, 215–221 (2012).
26. Bhushan, B. & Venkatesan, S. Effective mechanical properties of layered rough surfaces. *Thin Solid Films* **473**, 278–295 (2005).
27. Derjaguin, B. V. Molekulartheorie der äuβeren reibung. *Z. Phys.* **88**, 661–675 (1934).
28. Attard, P. Measurement and interpretation of elastic and viscoelastic properties with the atomic force microscope. *J. Phys.: Condens. Matter* **19**, 473201 (2007).

Acknowledgments

Author contributions

X.J.L. prepared the silicon dioxide films used in the measurement. R.I.R. performed experiments and analyzed the data. Y.L.Y., C.W. and R.I.R. discussed the results and contributed to the manuscript.

Additional information

Supplementary information accompanies this paper at http://www.nature.com/scientificreports

Competing financial interests: The authors declare no competing financial interests.

How to cite this article: Revilla, R.I., Li, X.-J., Yang, Y.-L. & Wang, C. Large Electric Field–Enhanced–Hardness Effect in a SiO_2 Film. *Sci. Rep.* **4**, 4523; DOI:10.1038/srep04523 (2014).